11-2012

Photocatalytic Activity Of Core/shell Semiconductor Nanocrystals Featuring Spatial Separation Of Charges

Dimuthu Perera

Ryan Lorek

Rony S. Khnayzer

Pavel Moroz

Timothy O'Connor

See next page for additional authors

THE JOURNAL OF PHYSICAL CHEMISTRY C

Article

pubs.acs.org/JPCC

Photocatalytic Activity of Core/Shell Semiconductor Nanocrystals Featuring Spatial Separation of Charges

Dimuthu Perera,[§] Ryan Lorek,[§] Rony S. Khnayzer,[†,‡] Pavel Moroz,[†,§] Timothy O'Connor,[§] Dmitry Khon,[⊥] Geoffrey Diederich,[§] Erich Kinder,[‡] Scott Lambright,[‡] Felix N. Castellano,[†,‡] and Mikhail Zamkov*[,†,§]

[†]The Center for Photochemical Sciences, [‡]Department of Chemistry, and [§]Department of Physics, Bowling Green State University, Bowling Green, Ohio 43403, United States

[⊥]Department of Chemistry and Biochemistry, St. Mary's University, One Camino Santa Maria, San Antonio, Texas 78228, United States

Supporting Information

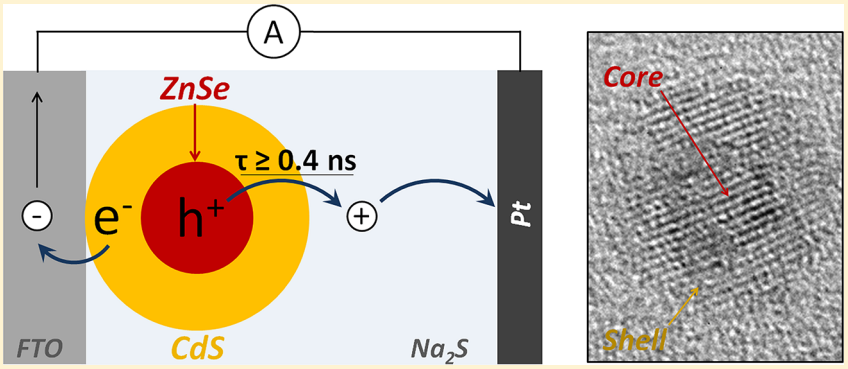

ABSTRACT: The present study investigates the photocatalytic activity of ZnSe/CdS core/shell semiconductor nanocrystals. These nanoparticles exhibit a spatial separation of photoinduced charges between the core and the shell domains, which makes them potentially viable for photocatalytic applications. Unfortunately, one of the excited charges remains inside the core semiconductor and thus cannot efficiently react with the external environment. Here, we explore this issue by investigating the mechanisms of hole extraction from the ZnSe core to the surface of the CdS shell. In particular, the effect of shell thickness in ZnSe/CdS core/shell nanocrystals on the ability of core-localized charges to perform oxidative reactions was determined. By using a combination of time-resolved spectroscopy and electrochemical techniques, we demonstrate that the use of hole-scavenging surfactants facilitates an efficient transfer of core-localized holes to the surface even in the case of shells exceeding 7 nm in thickness. These measurements further demonstrate that photoinduced holes can be extracted from the core faster than they recombine with shell-localized electrons, indicating that most of the absorbed energy in ZnSe/CdS nanocrystals can be used to drive catalytic reactions.

INTRODUCTION

Semiconductor nanocrystals (NCs) are emerging as a promising class of nanoscale materials for the development of artificial photocatalytic systems. The energy of excited states in these nanoparticles can be tuned continuously via nanoparticle size, which presents a unique opportunity for the design of nanostructures exhibiting a significant spatial separation of charges, an important property for a photocatalytic material. Furthermore, many semiconductor nanocrystals have a large extinction coefficient across the visible spectral range. This should facilitate the development of "solar powered" catalysts to drive chemical reactions with both electrons and holes having sufficient electric potentials to perform their respective catalytic functions. Owing to these benefits, single-phase semiconductor nanocrystals have been actively explored in a variety of photocatalytic applications.[1] It was not until recently, however, that advances in colloidal growth of more complex nanocrystal morphologies have finally unlocked a vast potential of nanostructured catalysts, resulting in the demonstration of novel material systems for hydrogen generation and decomposition of organic pollutants.[2−5]

To enhance the photoinduced separation of charges, nanocrystal catalysts are often constructed from two dissimilar semiconductor domains, which have complementary donor and acceptor functionalities.[6−9] Such a two-component architecture is typically optimized to ensure that electron and hole wave functions have minimal spatial overlap. This leads to the suppression of backward charge recombination enabling both

Received: September 7, 2012
Revised: October 11, 2012
Published: October 16, 2012

carriers to participate in catalytic reactions. Some representative examples of aforementioned two-domain structures include recently reported dot-in-a-rod,[10−15] tetrapod,[10,16,17] or barbell[18−20] composites comprising an electron-donating quantum dot component, which is coupled to one or more electron-accepting nanorod segments. Recent works have shown that these heteronanocrystals can drive a near-complete separation of photoinduced charges by relaying either electrons or holes to a metal catalyst (for example, Pt or Au) grown onto the donor or the acceptor semiconductor domain.[21−29]

Arguably, the simplest nanocrystal architecture capable of photoinduced charge separation is a core/shell arrangement of two semiconductor materials.[30] As was confirmed by a number of recent reports, excitation of core/shell NCs comprising ZnSe/CdS,[31,32] CdSe/CdTe,[33,34] or ZnTe/CdSe[35,36] semiconductor combinations results in the formation of weakly interacting electron−hole pairs, where both charges remain in the excited state long enough to share their energy with the external environment. Unfortunately, the utilization of nanocrystals with core/shell morphologies for catalytic applications is hampered by the fact that one of the carriers is confined to the core of the structure. As a result, the core-localized charge is not easily accessible for surface reactions and, instead, shares its energy with the semiconductor lattice through the process of photocorrosion. Recently, however, a number of reports utilizing ZnSe/CdS[29] and CdSe/CdS[28,37] dot-in-a-rod and ZnTe/CdSe[38] core/shell heteronanocrystals have indicated that if an outer layer is sufficiently thin and is modified with an appropriate charge-accepting moiety (e.g., 3-mercaptopropionic acid or phenothiazine molecules), core-localized holes can tunnel to the surface of the structure and be regenerated by a scavenging agent. What remains unclear is how the shell thickness in core/shell NCs affects the extraction of core-localized charges and whether it is at all possible to utilize the energy of the extracted carriers for chemical reactions on the surface.

Here we evaluate the photocatalytic activity of core/shell semiconductor nanocrystals by measuring the rate at which core-localized charges can be extracted to the surface of composite nanoparticles. By using ZnSe/CdS core/shell NCs as a model system of charge-separating nanocomposites, we demonstrate that photoinduced holes residing in the ZnSe domain can be promoted to nanoparticle surfaces in 0.4−10 ns, depending on the thickness of the CdS shell. This result indicates that both charges in core/shell NCs can be extracted to the surface faster than they recombine radiatively. To demonstrate that core-localized holes are capable of driving chemical reactions on nanoparticle surfaces, films of ZnSe/CdS nanocrystals were incorporated into an electrochemical cell, which was configured for the detection of extracted holes as photocurrent.

Overall, the present investigation highlights two important properties of type II core/shell semiconductor NCs, which are relevant to their catalytic applications. First, core-localized charges in nanocrystals with shells up to 7 nm thick can be extracted to the surface and therefore made available to perform chemical reactions. Second, surfactant-mediated removal of photoinduced charges from the semiconductor nanoparticle can significantly reduce the rate of semiconductor photocorrosion. This, in turn, suppresses the process of catalyst decomposition, thereby extending its operational lifetime.

EXPERIMENTAL SECTION

Chemicals. Oleylamine (tech., 70%, Aldrich), sulfur (99.999%, Acros), 1-octadecene (ODE, tech., 90%, Aldrich), cadmium oxide (CdO, 99.99%, Aldrich), octadecylamine (ODA, 90%, Fisher), oleic acid (OA, tech., 90%, Aldrich), tri-*n*-octylphosphine (TOP, 97%, Strem), tri-*n*-octylphosphine oxide (TOPO, 99%, Aldrich), *n*-octadecylphosphonic acid (ODPA, 98%, PCI Synthesis), *n*-hexylphosphonic acid (HPA, 98%, PCI Synthesis), hexadecylamine (HDA, tech., Fluka), 1,2-hexadecanediol (TCI), 11-mercaptoundecanoic acid (MUA, 95%, Aldrich), platinum(II) acetylacetonate (97%, Aldrich), tellurium powder (Te, −200 mesh, 99.8%, Aldrich), diethylzinc (Et_2Zn, 15 wt %, 1.1 M solution in toluene, Aldrich), selenium powder (Se, 200 mesh, Acros), hexane (anhydrous, 95%, Aldrich), methanol (anhydrous, 99.8%, Aldrich), ethanol (anhydrous, 95%, Aldrich), *tert*-butanol (99.7%, Aldrich), and toluene (anhydrous, 99.8%, Aldrich) were used as purchased. All reactions were performed under an argon atmosphere using standard Schlenk techniques unless otherwise stated.

ZnSe NCs. ZnSe NCs were synthesized according to the procedure reported by Cozzoli et al.[39] 7.0 g of ODA was degassed at 130 °C with stirring for 90 min in a three-neck flask. After degassing, the solution was switched to argon and heated to 300 °C. (It is important to use a wide exhaust vent as ODA vapors will resolidify at room temperature and clog narrow vents.) At this point, a selenium precursor prepared by dissolving 0.063 g of Se in 2.0 mL of degassed TOP through sonication under argon was injected into the reaction flask containing the degassed ODA. The mixture was then reheated to 300 °C. To initiate the NC growth, 1.0 mL of a 10% diethylzinc solution (10 wt % in hexane) was injected directly into the reaction flask, and the temperature was allowed to stabilize at 265 °C and kept at this level for the duration of the reaction. The growth was stopped in approximately 3−5 min when the position of the absorbance edge in growing nanocrystals reached λ = 360 nm. Prolonged growth of nanocrystals sometimes resulted in the formation of nanorods, which was not the desired morphology for ZnSe. After the growth stage, the flask was cooled down to 60 °C, 20 mL of methanol was added, and the flask was reheated back to 60 °C. For the initial washing cycle the mixture must be kept at above 55 °C prior to centrifuging to prevent the ODA from solidifying. NCs were precipitated with methanol, redispersed in chloroform, and stored in chloroform.

Synthesis of ZnSe/CdS Core/Shell. For the growth of CdS shells onto ZnSe seeds, a Cd precursor solution was prepared by dissolving 0.03 g of CdO, 0.6 mL of OA, and 5.4 mL of ODE at 290 °C under argon while stirring. Once a clear solution is obtained, the mixture was allowed to cool to room temperature. Similarly, a sulfur solution was prepared by heating 0.0077 g of sulfur in 6.0 mL of ODE to 200 °C under argon while stirring until clear and cooling to room temperature. In a three-neck flask, 1.5 g of ODA and 6.3 mL of ODE were combined and degassed at 120 °C for 30 min. After switching the flask to argon, 1 mL of ZnSe NC solution in chloroform, prepared in the first stage of the procedure, was added into the mixture, and the temperature was raised to 240 °C. The concentration of ZnSe seeds for the shell growth procedure was determined by setting the absorbance of the NC solution at the exciton shoulder ($\lambda \approx$ 360 nm) to 1.5 (as measured using a 1 mm thick cuvette)—approximately half the amount of NCs fabricated in the first stage. Once the

dx.doi.org/10.1021/jp308921s | J. Phys. Chem. C 2012, 116, 22786−22793

temperature of the reaction mixture reached 240 °C, 0.15 mL of the combined mixture of Cd and S precursor solutions was injected every 10 min. The growth of the CdS shell was monitored by measuring the NC emission. For instance, after the second injection, low-intensity red emission appeared due to CdS trap states. The continuous addition of precursors subsequently resulted in the onset of band gap emission at $\lambda \approx$ 450 nm, and after 90 min, strong green emission ($\lambda \approx$ 510−520 nm) was observed, at which point the reaction was stopped by raising the flask from the heating mantle. When the solution temperature reached 50 °C, 18 mL of ethanol was added to the flask and the solution was centrifuged to precipitate NCs, which were then redissolved in chloroform. After cleaning the NCs one more time by the addition of 18 mL of ethanol, the precipitate was dissolved in chloroform and stored.

Ligand Exchange. The original hydrophobic ligands on ZnSe/CdS NCs were exchanged with hydrophilic MUA using a method reported by Costi et al.[23] To this end, the solution of nanoparticles in 10−12 mL of chloroform was mixed with 10 mg of MUA. Subsequently, 4 mL of KOH solution (0.1 g of KOH in 20 mL of ultrapure water) was added, and the mixture was vigorously shaken until ZnSe/CdS NCs were transferred into the aqueous phase. The latter was separated and extracted one more time using 2 mL of aqueous KOH. Finally, MUA-capped NCs were precipitated with 10 mL of methanol and redissolved in 4 mL of ultrapure water.

Electrochemical Measurements. Linear sweep voltammetry was recorded using an Epsilon BASi workstation using a conventional three-electrode arrangement. In a quartz cubical photoelectrochemical cell equipped with home-built Teflon cap containing holes for electrode insertion at fixed positions, ∼20 mL of 0.1 mM Na_2S and 10 mM Na_2SO_4 electrolyte was added. The working electrode consisted of fluorine-doped tin oxide electrode (FTO) bearing the nanoparticle films. The reference electrode was Ag/AgCl prestored in 3 M NaCl, and the counter electrode consisted of a platinum wire. The cell was degassed by argon bubbling for 30 min before the experiment, and the headspace was maintained under argon flow during the measurements. The light source consisted of a 300 W Xe lamp equipped with a water filter to remove IR radiation and a 400 nm long pass filter to remove UV components and to selectively excite the semiconductor deposited on the FTO substrate. The excitation light was passed through a fiber bundle to a focusing lens producing ∼100 mW/cm^2 incident broadband light on the sample.

Characterization. UV−vis absorption and photoluminescence spectra were recorded using a Cary 50 scanning spectrophotometer and a Jobin-Yvon Fluorolog FL3-11 fluorescence spectrophotometer. High-resolution transmission electron microscopy measurements were carried out using JEOL 311UHR operated at 300 kV. Specimens were prepared by depositing a drop of nanoparticle solution in organic solvent onto a carbon-coated copper grid and allowing it to dry in air. X-ray powder diffraction (XRD) measurements were carried out on a Scintag XDS-2000 X-ray powder diffractometer. FL lifetime measurements were performed using a time-correlated single photon counting setup utilizing SPC-630 single-photon counting PCI card (Becker & Hickl GmbH), picosecond diode laser operating at 400 nm as an excitation source (Picoquant), and an id50 avalanche photodiode (Quantique).

Fluorescence Quantum Yield Measurements. The FL quantum yield of NC samples was determined relative to organic dyes with known emission efficiencies using the equation

$$QY_{NC} = QY_{Dye}\frac{I_{NC}}{I_{Dye}}\left(\frac{n_{NC}}{n_{Dye}}\right)^2\frac{1-10^{-A_{Dye}}}{1-10^{-A_{NC}}}$$

where I is the spectrally integrated fluorescence, n is the refractive index of the sample, and A is the optical absorbance of the sample at the excitation wavelength. The NC samples were excited using a 532 nm monochromatic laser (GS3230-20). Rhodamine B dye in ethanol with the emission at λ = 610 nm was used as a reference for QY measurements. The FL was detected using a home-built system comprising a Shamrock spectrograph and an Andor Newton EMCCD camera.

RESULTS AND DISCUSSION

The spatial separation of photoinduced charges in core/shell nanocrystals is generally expected when the energy minima of electron and hole states lie in the two different semiconductor domains (a type II system). Upon band gap excitation, such material arrangement creates a built-in electric field capable of driving excited carriers into the opposite sides of the core/shell interface, as illustrated in Figure 1. In this work, a ZnSe/CdS

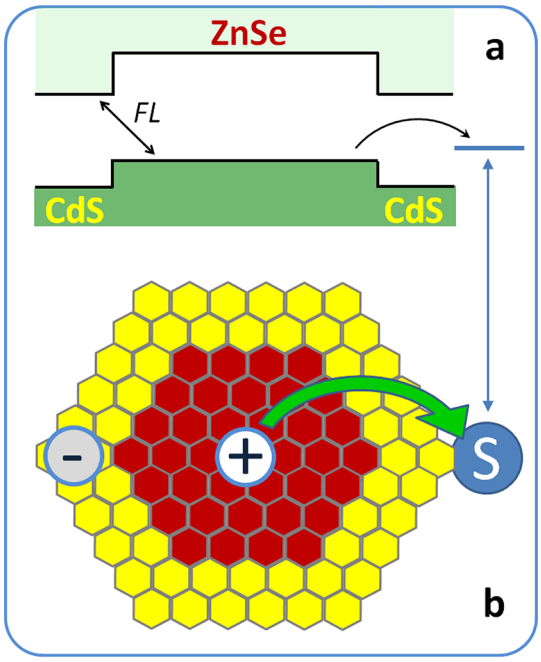

Figure 1. (a). Schematic illustration of the energy alignment between excited states at the interface of ZnSe/CdS core/shell NCs. The offset of CdS and ZnSe band edges causes photoinduced charges to localize in the opposite domains. (b). Schematic of the photoinduced charge separation in ZnSe/CdS core/shell NCs. The holes are confined inside the core domain and can be promoted to the surface (via tunneling) if the HOMO level of the surfactant lies above the ZnSe valence band.

semiconductor combination comprising a 2.9 nm ZnSe core capped with a CdS shell was chosen as a model system of a type II structure. According to previous reports,[32,40] photoexcitation of these nanoparticles results in the localization of photoinduced holes in the ZnSe and electrons in the CdS portions of the composite nanoparticle (Figure 1). The formation of spatially separated excited states is observed via the "spatially indirect" emission, for which the corresponding photon energy

dx.doi.org/10.1021/jp308921s | J. Phys. Chem. C 2012, 116, 22786−22793

falls below the band gap of either ZnSe or CdS materials (Figure 1a). Further evidence supporting the existence of charge-separated electron–hole pairs, $1S_e(CdS)1S_h(ZnSe)$, is provided by the relatively long fluorescence lifetime of spatially extended excitons (τ = 75 ns, see Figure 2d), which reflects a weak overlap of electron and hole wave functions across the type II interface.

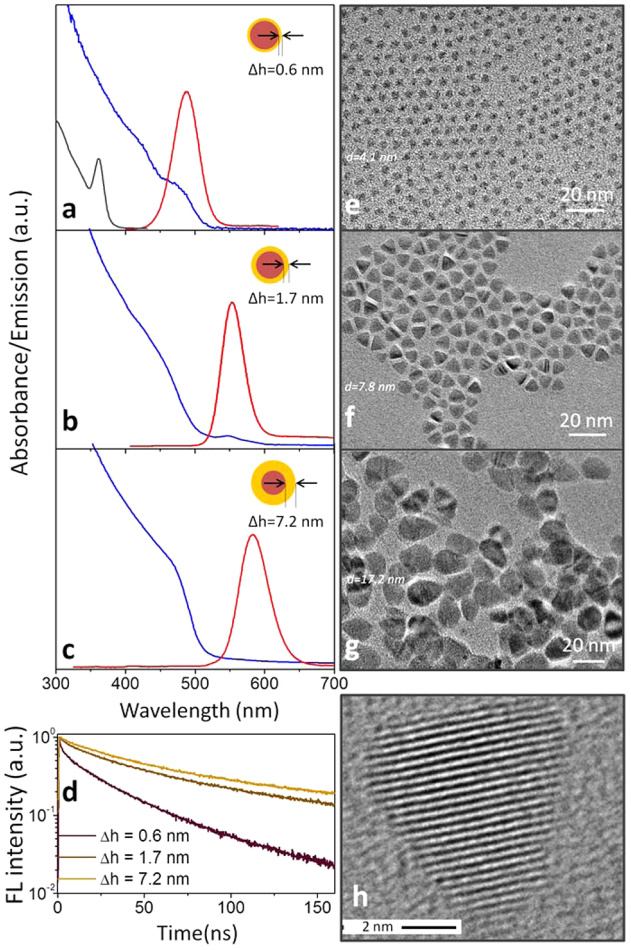

Figure 2. Optical and structural characterization of ZnSe/CdS NC samples representing different morphologies of the CdS shell. (a) Absorption and emission of 2.9 nm ZnSe NCs overcoated with a 0.6 nm CdS shell. The absorption profile of ZnSe core NCs is shown in gray. (b) Absorption and emission profile of 2.9 nm ZnSe NCs overcoated with a 1.7 nm CdS shell. (c) Absorption and emission profile of 2.9 nm ZnSe NCs overcoated with a 7.2 nm CdS shell. (d) Fluorescence intensity decay of the three types of core/shell NCs coated with hydrophobic ligands (oleic acid/TOPO). (e–g) TEM images of ZnSe/CdS core/shell NC samples with average diameters of 4.1 nm (e), 7.8 nm (f), and 17.2 nm (g). (h) A characteristic high-resolution TEM image of an isolated ZnSe/CdS NC.

Typically, the surfaces of as-prepared ZnSe/CdS nanocrystals are coated with long-chain amines or fatty acids that provide a substantial potential barrier to both electrons and holes shielding them from the external environment. Therefore, to facilitate the extraction of photoinduced holes from the core domain, the original ligands need to be replaced with an appropriate surface modifier, whose highest occupied molecular orbital (HOMO) level is situated above that of the ZnSe valence band edge.[41] One straightforward approach to achieve such surface modification relies on coating NCs with mercaptopropionic or mercaptoundecanoic acids (MPA and MUA, respectively).[42] These surface ligands are known to scavenge holes from zinc and cadmium chalcogenide nanocrystals, resulting in quenching of the band gap emission. As was demonstrated by an earlier work on MPA-coated CdSe NCs,[43] the suppression of the emission occurs due to the transfer of the photoinduced hole from CdSe NCs into a HOMO state of the MPA ligand. To achieve a similar level of hole extraction efficiency while providing an adequate stabilization of nanocrystals in aqueous solutions, longer-chain MUA molecules were employed in this study as a hole-scavenging surfactant.

The ZnSe-to-ligand hole transfer was calculated in this study from the measurements of the fluorescence intensity decay of "spatially indirect" excitons, $1S_e(CdS) \rightarrow 1S_h(ZnSe)$, as detailed in ref 44. Briefly, the FL lifetime, τ_{FL}, of MUA-capped ZnSe/CdS NCs is determined by the competition of the two processes: a slow-rate radiative decay (rate = Γ_R) corresponding to the $1S_e(CdS) \rightarrow 1S_h(ZnSe)$ band edge recombination and a nonradiative decay, which includes a slow-rate component associated with charge trapping on impurities and defects (Γ_{NR}^{trap}) and a fast-rate component associated with the transfer of holes to surface ligands ($\Gamma_{NR}^{transfer}$). Here, Γ denotes the amplitude contribution of a given deactivation pathway rate into the total rate of the process. With these considerations, the FL lifetime of the spatially indirect emission of MUA-capped ZnSe/CdS NCs, τ_{FL}, can be expressed as

$$\tau_{FL} = \tau_R \frac{\Gamma_R}{\Gamma_R + \Gamma_{NR}^{transfer} + \Gamma_{NR}^{trap}} \quad (1)$$

where τ_R is the radiative lifetime of $1S_e(CdS) \leftrightarrow 1S_h(ZnSe)$ transitions in ZnSe/CdS heteronanocrystals. Between the three processes contributing to the depletion of the excited carrier population, the ZnSe-to-ligand hole transfer is the fastest, $\Gamma_{NR}^{transfer} \gg (\Gamma_{NR}^{trap}, \Gamma_R)$. Indeed, an earlier study[29] has shown that when the hole transfer from the core domain to MUA ligands is energetically suppressed (for instance, when ZnTe semiconductor is used in the core domain instead of ZnSe), the emission lifetime of MUA-capped core/shell NCs increases by 1–2 orders of magnitude (τ = 68 ns). For ZnSe/CdS NCs, the core-to-ligand hole transfer is energetically allowed, which opens up an additional channel for carrier removal from the $1S_h(ZnSe)$ state, resulting in shorter emission lifetimes (τ < 1 ns). Under the assumption that trapping of carriers is much slower than the hole transfer process ($\Gamma_{NR}^{trap} \rightarrow 0$), the average hole transfer time, $\tau_{transfer}$, can be expressed as follows (see Supporting Information for details):

$$\tau_{transfer} = \tau_{FL}/(1 - (\tau_{FL}/\tau_R)) \quad (2)$$

Notably, the radiative lifetime of $1S_e(CdS)1S_h(ZnSe)$ excitons is a necessary parameter for calculating $\tau_{transfer}$. While the exact value of τ_R is unknown, a good approximation of $\tau_{transfer}$ can be obtained if τ_R is replaced with the FL lifetime of well-passivated nanocrystals (having original ligands).[44] To illustrate this point, we refer to Figure 3a showing the FL decay trace of MUA-capped ZnSe/CdS nanocrystals in water (red curve). The emission lifetime for these structures ($\tau \approx 0.44$ ns) is significantly shorter than the fluorescence lifetime of "spatially indirect" excitons in TOPO-capped ZnSe/CdS nanoparticles (>20 ns, see Figure 2d). Consequently, the photoinduced hole transfer to the MUA surface ligand, as estimated from eq 2, occurs in $\tau_{transfer} \approx 0.44/(1 - 0.44/20.00)$

dx.doi.org/10.1021/jp308921s | J. Phys. Chem. C 2012, 116, 22786–22793

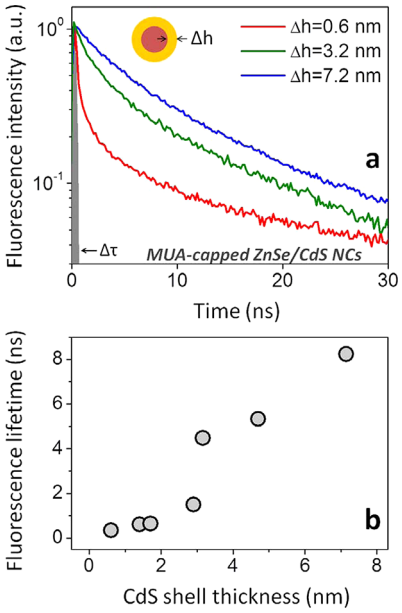

Figure 3. (a) Fluorescence lifetime of ZnSe/CdS NCs capped with hole-scavenging MUA ligands. Data are shown for three types of nanoparticles representing different thicknesses of the CdS shell: Δh = 0.6 nm (green), Δh = 3.2 nm (red), and Δh = 7.2 nm (blue). The increase in the FL lifetime for thick-shelled NCs is attributed to a slower transfer of photoinduced holes across the CdS layer. (b) Dependence of Fl lifetime on the thickness of the CdS shell in MUA-capped ZnSe/CdS NCs.

≈ 0.449 ps. If our assumption regarding the radiative lifetime was not correct and τ_R is much greater than the FL lifetime of TOPO-coated NCs, then the actual $\tau_{transfer}$ would be found in the 0.440−0.449 ps range, which constitutes less than 2% of the experimental uncertainty.

To understand how the thickness of the shell in core/shell NCs affects the transfer of holes to the surface, we have fabricated a series of ZnSe/CdS NCs representing an increasing number of CdS monolayers (MLs). Figure 2 shows three examples of such ZnSe/CdS structures fabricated using the same ZnSe core diameter (d = 2.9 nm) and CdS shells measuring Δh = 0.6 nm (e), Δh = 1.7 nm (f), and Δh = 7.2 nm (g) in thickness. As evident from the high-resolution transmission electron microscope (TEM) image in Figure 2h, the shell grew around the core in pyramid-type morphology without noticeable lattice defects. The high quality of the semiconductor interface was attributed to a relatively low lattice mismatch between ZnSe and CdS crystal phases (strain ≈ 2.7%). The formation of the shell was confirmed by the characteristic shift of Bragg lines in the X-ray powder diffraction spectra of ZnSe/CdS NCs (see Figure SF1).

The character of electron−hole localization in fabricated ZnSe/CdS NCs was substantiated based on steady-state absorption and emission characteristics of these colloids, as summarized in Figures 2a−d. According to Figure 2b, the deposition of a thin, 1.8-monolayer CdS shell (Δh = 0.6 nm) results in broadening of the ZnSe band edge transition (λ = 360 nm) as well as a simultaneous growth of the CdS excitonic edge at $\lambda \approx$ 475 nm, attributed to the lowest energy $1S(e)-1S_{3/2}(h)$ excitation in the CdS domain. The deposition of the CdS shell was also accompanied by the onset of a new absorption feature, whose spectral position was red-shifted from the CdS edge by ~50 nm. This absorption maximum arises from the "spatially indirect" transition of excited carriers, which involves excitation of the ZnSe valence electrons into the conduction band of CdS, as illustrated in Figure 1a. This process is commonly observed in type II semiconductor heteronanocrystals and has been extensively characterized in earlier reports.[20,31,32] As expected, the spectral position of $1S_h$(ZnSe) → $1S_e$(CdS) absorption maximum was found to correlate with the "spatially indirect" fluorescence ($\lambda \approx$ 480 nm), which dominated the emission spectra of ZnSe/CdS core/shell nanocrystals. The interdomain (CdS(e) ↔ ZnSe(h)) character of the observed emission peak is corroborated by the comparatively low energy of associated photons, which falls below the band gap of both ZnSe and CdS semiconductor components, and the relatively long radiative lifetime of the $1S_e$(CdS) → $1S_h$(ZnSe) excited state (see Figure 2d).

The deposition of a medium (Δh = 1.7 nm) and a thick CdS shell (Δh = 7.2 nm) onto ZnSe core NCs was accompanied by broadening of the CdS excitonic band edge in the absorption spectrum (Figure 2c) reflecting the nanoparticle growth beyond the CdS exciton Bohr radius (R = 2.9 nm).[45] The "spatially indirect" absorption feature at λ = 550 nm has also undergone substantial broadening in thick-shell nanoparticles (Δh = 7.2 nm) due to a possible alloying at the interface of ZnSe and CdS semiconductors, which corresponds to a 2.7% lattice strain. The suppression of the type II absorption feature is commonly observed in core/shell structures with a greater lattice mismatch (e.g., CdSe/CdTe where the strain exceeds 5%) but could also be manifested in low-strain ZnSe/CdS structures when the shell domain becomes particularly large.

In addition to absorption changes, the growth of a thick CdS shell around the ZnSe core has produced noticeable changes in the emission profile of core/shell NCs. According to Figures 2b and 2c, the "spatially indirect" fluorescence peak, originally centered at $\lambda \approx$ 480 nm (for Δh = 0.6 nm), underwent a continuous red-shift with a growing number of shell monolayers, ultimately reaching a saturation value of λ = 587 nm (for Δh = 7.2 nm). A positive correlation between the peak spectral position and the shell thickness was attributed to the fact that the energy of photoinduced electrons residing in the CdS domain is lowered with increasing Δh due to the loss of carrier confinement in the shell. Likewise, thickening of a CdS shell resulted in noticeable changes in the emission lifetime of ZnSe/CdS nanoparticles, which has increased from 21 ns for Δh = 0.6 nm to 76 ns for Δh = 7.2 nm (Figure 2d). This phenomenon is indicative of a diminishing overlap between electron and hole wave functions in nanocrystals with relatively thick shells.

To determine the rate of hole extraction from the core of ZnSe/CdS NCs, the original ligands on the nanoparticle surfaces were replaced with hole-scavenging MUA molecules. The ligand exchange step was accompanied by a significant suppression of the NC emission (due to ZnSe to MUA hole transfer) and a corresponding 10−100-fold drop in the $1S_e$(CdS)$1S_h$(ZnSe) exciton lifetime, as illustrated in Figure 3a. To ensure that the emission intensity decay traces reflect only the "spatially indirect" recombination of charges and exclude contributions from CdS trap states (650 nm < λ < 900 nm, see Figure SF2), NC emission was filtered to allow the 450−630 nm spectral band only. The use of a bandpass filter in this case allows blocking most of the photons originating from surface traps. While the presence of a trapped charge can also affect the recombination dynamics of "spatially indirect" photons, the resulting trap−electron−hole trion states are

dx.doi.org/10.1021/jp308921s | J. Phys. Chem. C 2012, 116, 22786−22793

expected to decay via nonradiative Auger processes, which do not directly contribute into the observed emission. The possible enhancement of the nonradiative decay rate due to Auger recombination contributes into the uncertainty of the recombination rate,[46] which ultimately amount to less than 2% of the experimental error (as demonstrated by an above calculation of $\tau_{transfer}$ from eq 2).

By comparing the emission lifetimes of MUA-capped nanoparticles with those containing original (nonpolar) ligands, it was possible to quantitatively evaluate the hole transfer rates using eq 2. Since τ_{FL} of MUA-capped NCs were substantially smaller than τ_R, the values of $\tau_{transfer}$ were only 1−2% above the corresponding τ_{FL} (see Table ST1 in Supporting Information). Here we assume that the radiative rate of exciton decay in ZnSe/CdS NCs was not substantially reduced upon ligand exchange (due to the loss of crystallinity, for example[41]). The constancy of τ_R can be verified by comparing the intrinsic radiative lifetimes, $\tau_R = \tau_{FL}/\Phi$ (where Φ is the FL quantum yield), between MUA- and OA-capped nanoparticles, as shown in Table ST2. Since the τ_{FL}/Φ ratio remains approximately the same for both types of surface passivations, we conclude that the reduction of the FL lifetime accompanying the OA → MUA ligand exchange is not caused by the decreased τ_R but rather reflects the loss of valence holes due to charge transfer to MUA.

According to Figure 3b, increasing the shell thickness in MUA-capped ZnSe/CdS NCs from 0.6 to 2.9 nm resulted in the enhancement of $\tau_{transfer}$ from 0.44 to 1.5 ns. A slower transfer of the photoinduced hole in this case is attributed to the augmented energetic barrier of a 2.9 nm CdS shell separating the potential minima of the photoinduced hole in the ZnSe and MUA domains. Indeed, a thicker CdS shell reduces the overlap between the hole wave function in ZnSe and the HOMO state of a surface ligand, thus lowering the rate of hole transfer to MUA. This trend is further confirmed by the observation of increased FL lifetime in MUA-capped ZnSe/CdS NCs comprising a 7.2 nm shell. In this case, the hole transfer time was determined to be 8.2 ns. The effect of the CdS shell thickness on the ZnSe → MUA hole transfer time is summarized in Figure 3b. The observed lifetime data indicate that the hole transit time is inversely proportional to the shell thickness. As expected, the highest rate of hole transfer to the surface ligand was observed for the case of the thinnest CdS shell (τ = 0.44 ns; Δh = 0.6 nm), whereas nanocrystals with the thickest shell (Δh > 7 nm) showed the lowest transfer rate.

The observed dependence of the hole transfer rate on the shell thickness highlights an interesting property of ZnSe/CdS core/shell NCs, which carries potential benefits for catalytic applications of these nanoparticles. As follows from Figure 3b, even in the case of a 20-monolayer shell (Δh = 7.2 nm) covering the surface of ZnSe NCs, the photoinduced hole can be extracted to the surface of the nanoparticle faster than it recombines with the shell-localized electron. Consequently, both excited carriers are likely to be preserved during the hole extraction step. For example, in the case of a 3.2 nm thick CdS shell, the hole transit time is 4.5 ns, while the FL lifetime of an electron−hole pair for these structures is 60 ns (see Figure 2d). Therefore, one can estimate that 100 exp(−4.5 ns/60 ns)% ≈ 93% of photoinduced holes in these nanoparticles will be transferred to the surface ligand without losing their oxidative energy through a carrier recombination process. Amazingly, even for nanoparticles comprising rather thick shells (>15 ML), more than 85% of photoinduced holes are expected to reach the surface. It is unclear, however, to what extent the surface localization of both carriers affects their recombination rates. This question is particularly difficult to answer in light of the fact that in many functional catalytic systems the two surface charges are localized within their designated catalytic domains (Pt, Au, cobalt phosphate "Co-Pi"), in which case the recombination rate is primarily determined by the morphology of the nanostructure. Further studies will need to be conducted to investigate this interesting issue.

If, in fact, photoinduced holes are extracted from the core domain of core/shell nanoparticles, one would expect to see some evidence of their chemical activity in a suitable environment. Here, we evaluate the photocatalytic performance of extracted holes, by incorporating thin films of ZnSe/CdS nanocrystals into an electrochemical assembly, as shown in Figure 4a. The electrical contacts consist of fluorine doped tin

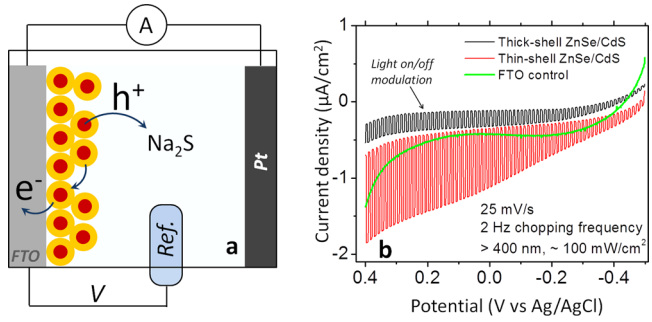

Figure 4. (a) A diagram of an electrochemical cell consisting of a ZnSe/CdS nanoparticle/FTO working electrode, Ag/AgCl reference electrode, and Pt counter electrode. (b) Linear sweep voltammetry of the two cells comprising thin-shell (Δh = 0.6 nm, red curve) and thick-shell (Δh = 7.2 nm, black curve) nanocrystal film working electrodes. The stronger photoresponse of the thin-shell samples is attributed to faster hole extraction to the surface.

oxide (FTO)-covered glass (anode), which supports the nanocrystal film, Ag/AgCl reference electrode, and a Pt cathode. Upon photoexcitation of ZnSe/CdS films, photoinduced electrons are promoted to the Pt electrode through a circuit, while holes are scavenged by a polysulfide electrolyte (Na_2S/Na_2SO_4). In this configuration, the photocurrent is proportional to the density of holes on the surface of core/shell NCs, such that the cell photocurrent can serve as a measure of the relative hole catalytic activity. Since we are merely interested in studying the photoanode, the electrolyte composition was chosen such that any polarization at the Pt electrode was compensated by the three-electrode arrangement. To perform electrochemical measurements, the NC films were optically excited using a white light source. A 400 nm high-pass filter was used to prevent direct excitation of the FTO layer, allowing for the cell current to be generated exclusively by NCs in the film.

To fabricate a nanocrystal film for electrochemical measurements, we used a recently reported semiconductor matrix encapsulated nanocrystal array (SMENA) approach, which allows incorporating ligand-free semiconductor NCs into all-inorganic matrices.[47] To this end, core/shell NCs were spin-coated onto a substrate and capped with thermally degradable ligands (MPA). The film was subsequently heated to about 150 °C in order to remove the organic phase and promote a mild fusion of neighboring shells. Upon heating, the surfaces of nanocrystals lose passivation and become charged, which

dx.doi.org/10.1021/jp308921s | J. Phys. Chem. C 2012, 116, 22786−22793

facilitates the charge-transfer reaction between the polysulfide electrolyte and the semiconductor. It should be noted that the removal of surface ligands enhances the density of trap states on the CdS surface as well. This is expected to suppress the flow of electrons toward the cathode, ultimately reducing the cell current. Fortunately, the trap-related reduction of the photoinduced current does not pose a significant issue since the present study focuses primarily on the relative comparison of photocurrents, which elucidates the qualitative behavior of the system.

The photocurrents of the cells fabricated from thin-shell (red) and thick-shell (blue) ZnSe/CdS nanoparticle films are plotted in Figure 4b versus the reference electrode voltage. For both samples, switching of the illumination light on and off results in the modulation of the photocurrent value, indicating that both charge types induced by the excitation light contribute into the electrical current. The amplitude of this contribution (for the fixed concentration of Na_2S) is proportional to the modulation signal, which drops off when $V_{ref} < -0.6$ V. The associated overpotential of ~0.6 eV is roughly the energy difference between HOMO of ZnSe and valence band edge of Pt. The observed current modulation in Figure 4b confirms the aforementioned hypothesis that core-localized charges can engage in the reaction on the surface of core/shell NCs even when the shell thickness is relatively thick (up to 7 nm).

According to Figure 4b, the amplitude of the photocurrent modulation for films containing thin-shell ZnSe/CdS nanocrystals (Δh = 0.6 nm) is about 3−4 times greater than that of thick-shell (Δh = 7.2 nm) NC films. This trend was reproducible over a large set of samples, allowing us to exclude effects of electrolyte concentration and sample preparation. Furthermore, the electrical responses of both films were normalized in relation to the film's optical density, indicating that the observed difference in the on/off photocurrent arises mainly due to the effect of the CdS shell thickness. The greater current observed in thin-shell films can be explained in terms of more efficient tunneling of photoinduced holes from ZnSe cores into the electrolyte material. Indeed, holes that travel faster to nanoparticle surfaces are less likely to be consumed through side reactions and are more likely to contribute into the cell current. We should note that this conclusion is based on the assumption that regeneration of surface charges is faster than the hole transition time. To verify this premise, films of pure CdS NCs were also investigated in an electrochemical cell. If the polysulfide electrolyte does provide a fast regeneration of holes (that are already on the surface), then it is reasonable to expect that nanocrystals without core-localization of charges should exhibit the most prominent photoresponse. For instance, a film of pure CdS NCs should give rise to a stronger photocurrent than ZnSe/CdS core/shell NCs, since in the former case holes are immediately available for regeneration. A comparison of the photocurrent amplitudes between ZnSe/CdS and CdS nanoparticle films confirms this hypothesis. According to Figure SF3, all-CdS films show a somewhat stronger modulation signal. This result allows us to conclude that scavenging of surface holes is faster than the hole transfer time and the stronger photocurrent in thin-shell ZnSe/CdS NC films can be attributed to faster tunneling of holes to the surface.

In summary, the catalytic activity of ZnSe/CdS core/shell semiconductor NCs was evaluated using a combination of electrochemical and fluorescence lifetime measurements. Our study demonstrates that both core- and shell-localized electrical charges can be efficiently extracted to the surface of the nanoparticle where they can exchange energy with the external environment. In particular, we show that the transfer of photoinduced charges from the core domain to the surface of the core/shell nanocrystals is approximately an order of magnitude faster than electron−hole recombination time. Consequently, a significant fraction of photoinduced electrical charges in core/shell NCs is available to drive catalytic reactions. The latter premise was confirmed in this study through the investigation of ZnSe/CdS catalytic activity in an electrochemical cell.

■ ASSOCIATED CONTENT

Supporting Information

Details of materials syntheses, X-ray power diffraction data (XRD), additional TEM images, and FT-IR spectra. This material is available free of charge via the Internet at http://pubs.acs.org.

■ AUTHOR INFORMATION

Corresponding Author

*E-mail zamkovm@bgsu.edu.

Notes

The authors declare no competing financial interest.

■ ACKNOWLEDGMENTS

This work was supported by the NSF under Awards CHE-1112227 (M.Z.) and CHE-1012487 (F.N.C.). Development of solid films was also supported by the NSF under Award CBET-1236355 (M.Z.). We gratefully acknowledge the state of Ohio OBOR "Material Networks" program and Bowling Green State University for financial support.

■ REFERENCES

(1) Maeda, K.; Domen, K. Photocatalytic Water Splitting: Recent Progress and Future Challenges. *J. Phys. Chem. Lett.* **2010**, *1*, 2655−2661.

(2) Kamat, P. V. Manipulation of Charge Transfer Across Semiconductor Interface. A Criterion That Cannot Be Ignored in Photocatalyst Design. *J. Phys. Chem. Lett.* **2012**, *3*, 663−672.

(3) Ruberu, T. P. A.; Nelson, N. C.; Slowing, I. I.; Vela, J. Selective Alcohol Dehydrogenation and Hydrogenolysis with Semiconductor-Metal Photocatalysts: Toward Solar-to-Chemical Energy Conversion of Biomass-Relevant Substrates. *J. Phys. Chem. Lett.* **2012**, *3*, 2798−2802.

(4) Shemesh, Y.; Macdonald, J. E.; Menagen, G.; Banin, U. Synthesis and Photocatalytic Properties of a Family of CdS-PdX Hybrid Nanoparticles. *Angew. Chem., Int. Ed.* **2011**, *50*, 1185−1189.

(5) Chen, X.; Shen, S.; Guo, L.; Mao, S. S. Semiconductor-Based Photocatalytic Hydrogen Generation. *Chem. Rev.* **2010**, *110*, 6503−6570.

(6) Donega, C. D. Synthesis and Properties of Colloidal Heteronanocrystals. *Chem. Soc. Rev.* **2011**, *40*, 1512−1546.

(7) Carbone, L.; Cozzoli, P. D. Colloidal Heterostructured Nanocrystals: Synthesis and Growth Mechanisms. *Nano Today* **2010**, *5*, 449−493.

(8) She, C.; Demortière, A.; Schevchenko, E. V.; Pelton, M. Using shape to control photoluminescence from CdSe/CdS core/shell nanorods. *J. Phys. Chem. Lett.* **2011**, *2*, 1469.

(9) Lo, S. S.; Mirkovic, T.; Chuang, C. H.; Burda, C.; Scholes, G. D. Emergent Properties Resulting from Type-II Band Alignment in Semiconductor Nanoheterostructures. *Adv. Mater.* **2011**, *23*, 180−197.

(10) Carbone, L.; Nobile, C.; de Giorgi, M.; Sala, F. D.; Morello, G.; Pompa, P.; Hytch, M.; Snoeck, E.; Fiore, A.; Franchini, I. R.; Nadasan,

M.; Silvestre, A. F.; Chiodo, L.; Kudera, S.; Cingolani, R.; Krahne, R.; Manna, L. Synthesis and Micrometer-Scale Assembly of Colloidal CdSe/CdS Nanorods Prepared by a Seeded Growth Approach. *Nano Lett.* **2007**, *7*, 2942−2950.
(11) Ruberu, T. P. A.; Vela, J. Expanding the One-Dimensional CdS-CdSe Composition Landscape: Axially Anisotropic $CdS_{1-x}Se_x$ Nanorods. *ACS Nano* **2011**, *5*, 5775−5784.
(12) Dorfs, D.; Salant, A.; Popov, I.; Banin, U. ZnSe Quantum Dots Within CdS Nanorods: A Seeded-Growth Type-II System. *Small* **2008**, *4*, 1319−1323.
(13) Lo, S. S.; Khan, Y.; Jones, M.; Scholes, G. D. Temperature and solvent dependence of CdSe/CdTe heterostructure nanorod spectra. *J. Chem. Phys.* **2009**, *131*, 084714.
(14) Kumar, S.; Jones, M.; Lo, S. S.; Scholes, G. D. Nanorod heterostructures showing photoinduced charge separation. *Small* **2007**, *3*, 1633−1639.
(15) Hewa-Kasakarage, N. N.; Kirsanova, M.; Nemchinov, A.; Schmall, N.; El-Khoury, P. Z.; Tarnovsky, A. N.; Zamkov, M. Radiative Recombination of Spatially Extended Excitons in (ZnSe/CdS)/CdS Heterostructured Nanorods. *J. Am. Chem. Soc.* **2009**, *131*, 1328−1334.
(16) Carbone, L.; Kudera, S.; Carlino, E.; Parak, W. J.; Giannini, C.; Cingolani, R.; Manna, L. Multiple wurtzite twinning in CdTe nanocrystals induced by methylphosphonic acid. *J. Am. Chem. Soc.* **2006**, *128*, 748−755.
(17) Milliron, D. J.; Hughes, S. M.; Cui, Y.; Manna, L.; Li, J.; Wang, L.; Alivisatos, A. P. Colloidal nanocrystal heterostructures with linear and branched topology. *Nature* **2004**, *430*, 190−195.
(18) Shieh, F.; Saunders, A. E.; Korgel, B. A. General Shape Control of Colloidal CdS, CdSe, CdTe Quantum Rods and Quantum Rod Heterostructures. *J. Phys. Chem. B* **2005**, *109*, 8538−8542.
(19) Halpert, J. E.; Porter, V. J.; Zimmer, J. P.; Bawendi, M. G. Synthesis of CdSe/CdTe Nanobarbells. *J. Am. Chem. Soc.* **2006**, *128*, 12590−12591.
(20) Kirsanova, M.; Nemchinov, A.; Hewa-Kasakarage, N. N.; Schmall, N.; Zamkov, M. Synthesis of ZnSe/CdS/ZnSe nano-barbells showing photoinduced charge separation. *Chem. Mater.* **2009**, *21*, 4305−4309.
(21) Harris, C.; Kamat, P. V. Photocatalytic Events of CdSe Quantum Dots in Confined Media. Electrodic Behavior of Coupled Platinum Nanoparticles. *ACS Nano* **2010**, *4*, 7321−7330.
(22) Mokari, T.; Rothenberg, E.; Popov, I.; Costi, R.; Banin, U. Selective Growth of Metal Tips onto Semiconductor Quantum Rods and Tetrapods. *Science* **2004**, *304*, 1787−1790.
(23) Costi, R.; Saunders, A. E.; Elmalem, E.; Salant, A.; Banin, U. Visible Light-Induced Charge Retention and Photocatalysis with Hybrid CdSe−Au Nanodumbbells. *Nano Lett.* **2008**, *8*, 637−641.
(24) Khon, E.; Mereshchenko, A.; Tarnovsky, A.; Acharya, K.; Klinkova, A.; Hewa-Kasakarage, N.; Nemitz, I.; Zamkov, M. Suppression of the Plasmon Resonance in Au/CdS Colloidal Nanocomposites. *Nano Lett.* **2011**, *11*, 1792−1799.
(25) Bao, N.; Shen, L.; Takata, T.; Domen, K. Self-Templated Synthesis of Nanoporous CdS Nanostructures for Highly Efficient Photocatalytic Hydrogen Production under Visible Light. *Chem. Mater.* **2008**, *20*, 110−117.
(26) Elmalem, E.; Saunders, A. E.; Costi, R.; Salant, A.; Banin, U. Growth of Photocatalytic CdSe−Pt Nanorods and Nanonets. *Adv. Mater.* **2008**, *20*, 4312−4317.
(27) Berr, M.; Vaneski, A.; Susha, A. S.; Rodríguez-Fernández, J.; Döblinger, M.; Jäckel, F.; Rogach, A. L.; Feldmann, J. Colloidal CdS nanorods Decorated with Subnanometer Sized Pt Clusters for Photocatalytic Hydrogen Generation. *J. Appl. Phys. Lett.* **2010**, *97*, 093108.
(28) Amirav, L.; Alivisatos, P. A. Photocatalytic Hydrogen Production with Tunable Nanorod Heterostructures. *J. Phys. Chem. Lett.* **2010**, *1*, 1051−1054.
(29) Acharya, K. P.; Khnayzer, R. S.; O'Connor, T.; Diederich, G.; Kirsanova, M.; Klinkova, A.; Roth, D.; Kinder, E.; Imboden, M.; Zamkov, M. The Role of Hole Localization in Sacrificial Hydrogen Production by Semiconductor−Metal Heterostructured Nanocrystals. *Nano Lett.* **2011**, *11*, 2919−2926.
(30) Reiss, P.; Protiere, M.; Li, L. Core/Shell Semiconductor Nanocrystals. *Small* **2009**, *5*, 154−168.
(31) Ivanov, S. A.; Piryatinski, A.; Nanda, J.; Tretiak, S.; Zavadil, K. R.; Wallace, W. O.; Werder, D.; Klimov, V. I. Type-II Core/Shell CdS/ZnSe Nanocrystals: Synthesis, Electronic Structures, and Spectroscopic Properties. *J. Am. Chem. Soc.* **2007**, *129*, 11708−11719.
(32) Nemchinov, A.; Kirsanova, M.; Hewa-Kasakarage, N. N.; Zamkov, M. Synthesis and Characterization of Type II ZnSe/CdS Core/Shell Nanocrystals. *J. Phys. Chem. C* **2008**, *112*, 9301−9307.
(33) Kim, S.; Fisher, B.; Eisler, H. J.; Bawendi, M. Type-II Quantum Dots: CdTe/CdSe(Core/Shell) and CdSe/ZnTe(Core/Shell) Heterostructures. *J. Am. Chem. Soc.* **2003**, *125*, 11466−11467.
(34) Donegá, C. M. Formation of Nanoscale Spatially Indirect Excitons: Evolution of the Type-II Optical Character of CdTe/CdSe Heteronanocrystals. *Phys. Rev. B* **2010**, *81*, 165303.
(35) Xie, R.; Zhong, X.; Basché, T. Synthesis, Characterization, and Spectroscopy of Type-II Core/Shell Semiconductor Nanocrystals with ZnTe Cores. *Adv. Mater.* **2005**, *17*, 2741−2745.
(36) Cheng, C. T.; Chen, C. Y.; Lai, C. W.; Liu, W. H.; Pu, S. C.; Chou, P. T.; Chou, Y. H.; Chiu, H. T. Syntheses and Photophysical Properties of Type-II CdSe/ZnTe/ZnS (core/shell/shell) Quantum Dots. *J. Mater. Chem.* **2005**, *15*, 3409−3414.
(37) Brown, K. A.; Wilker, M. B.; Boehm, M.; Dukovic, G.; King, P. W. Characterization of Photochemical Processes for H_2 Production by CdS Nanorod−[FeFe] Hydrogenase Complexes. *J. Am. Chem. Soc.* **2012**, *134*, 5627−5636.
(38) Jiang, Z. J.; Kelley, D. F. Effects of Inhomogeneous Shell Thickness in the Charge Transfer Dynamics of ZnTe/CdSe Nanocrystals. *J. Phys. Chem. C* **2012**, *116*, 12958−12968.
(39) Cozzoli, P. D.; Manna, L.; Curri, M. L.; Kudera, S.; Giannini, C.; Striccoli, M.; Agostiano, A. Shape and Phase Control of Colloidal ZnSe Nanocrystals. *Chem. Mater.* **2005**, *17*, 1296−1306.
(40) Steiner, D.; Dorfs, D.; Banin, U.; Della Sala, F.; Manna, L.; Millo, O. Determination of Band Offsets in Heterostructured Colloidal Nanorods Using Scanning Tunneling Spectroscopy. *Nano Lett.* **2008**, *8*, 2954−2958.
(41) Liu, D.; Snee, P. T. Water-Soluble Semiconductor Nanocrystals Cap Exchanged with Metalated Ligands. *ACS Nano* **2011**, *5*, 546−550.
(42) Sperling, R. A.; Parak, W. J. Surface modification, functionalization and bioconjugation of colloidal inorganic nanoparticles. *Philos. Trans. R. Soc., A* **2010**, *368*, 1333−1383.
(43) Völker, J.; Zhou, X. Y.; Ma, X.; Flessau, S.; Lin, H. W.; Schmittel, M.; Mews, A. Semiconductor Nanocrystals with Adjustable Hole Acceptors: Tuning the Fluorescence Intensity by Metal−Ion Binding. *Angew. Chem., Int. Ed.* **2010**, *49*, 6865−6868.
(44) O'Connor, T.; Panov, M.; Mereshchenko, A.; Tarnovsky, A. N.; Lorek, R.; Perera, D.; Diederich, G.; Lambright, S.; Moroz, P.; Zamkov, M. The Effect of the Charge-Separating Interface on Exciton Dynamics in Photocatalytic Colloidal Heteronanocrystals. *ACS Nano* **2012**, *6*, 8156−8165.
(45) Wang, Y.; Herron, N. Nanometer-sized Semiconductor Clusters: Materials Synthesis, Quantum Size Effects, and Photophysical Properties. *J. Phys. Chem.* **1991**, *95*, 525−532.
(46) Tagliazucchi, M.; Tice, D. B.; Sweeney, C. M.; Morris-Cohen, A. J.; Weiss, E. A. Ligand-controlled rates of photoinduced electron transfer in hybrid CdSe nanocrystal/poly(viologen) films. *ACS Nano* **2011**, *5*, 9907−9917.
(47) Kinder, E.; Moroz, P.; Diederich, G.; Johnson, A.; Kirsanova, M.; Nemchinov, A.; O'Connor, T.; Roth, D.; Zamkov, M. Fabrication of All-Inorganic Nanocrystal Solids through Matrix Encapsulation of Nanocrystal Arrays. *J. Am. Chem. Soc.* **2011**, *133*, 20488−20499.